Fuel 331 (2023) 125840

Contents lists available at ScienceDirect

Fuel

journal homepage: www.elsevier.com/locate/fuel

Full length article

The effect of turbulence on the conversion of coal under blast furnace raceway conditions

Eva-Maria Wartha [a,*], Nils Erland Haugen [b,c], Ewa Karchniwy [b], Markus Bösenhofer [a,d], Michael Harasek [a], Terese Løvås [e]

[a] TU Wien, Institute of Chemical, Environmental and Bioscience Engineering, Getreidemarkt 9/166, 1060 Vienna, Austria
[b] SINTEF Energi A.S., Sem Saelands vei 11, 7034 Trondheim, Norway
[c] Energy Engineering, Div. Energy Science, Luleå, University of Technology, 97187 Luleå, Sweden
[d] K1-Met GmbH, Area 4 - Simulation and Analyses, Stahlstrasse 14, BG 88, 4020 Linz, Austria
[e] Department of Energy and Process Engineering, Norwegian University of Science and Technology, Kolbjørn Hejes vei 1B, 7034 Trondheim, Norway

ARTICLE INFO

Keywords:
Coal combustion
Blast furnace
Turbulence effects
Kinetic-diffusion limited
Computational fluid dynamics

ABSTRACT

The main production route for steel in Europe is still via the blast furnace. Computational fluid dynamics (CFD) can be used to analyze the process virtually and thus improve its performance. Different reducing agents can be used to (partially) substitute the coke and consequently reduce overall emissions. To analyze different reducing agents effectively using CFD, their conversion process has to be modeled accurately. Under certain conditions, coal particles can cluster as the result of turbulence effects, which further reduces the mass transfer to the coal surface and consequently the conversion rate. We analyze the effect of turbulence under blast furnace raceway conditions on the conversion of coal particles and on the overall burnout. The model is applied in RANS to polydisperse particle systems and this is then compared to the simplified monodisperse assumption. Additionally, the model is extended by adding gasification reactions. Overall, we find that the turbulent effects on coal conversion are significant under blast furnace raceway conditions and should be considered in further simulations. Furthermore, we show that an a-priori assessment is difficult because the analysis via averaged quantities is impractical due to a strong variation of conditions in the furnace. Therefore, the effects of turbulence need to be correlated to the regions of conversion.

1. Introduction

Blast furnaces together with basic oxygen furnaces account for around 60% of current steel production in Europe [1]. Due to its very large energy consumption and high CO_2 emissions, the process is subject to ongoing improvements. Computational fluid dynamics (CFD) can help to better understand the process and obtain detailed information about the process conditions inside the blast furnace. Reducing agents can be supplied in the blast furnace raceway zone to reduce coke consumption [2,3]. Fig. 1 shows a schematic blast furnace with its in- and outflows and the raceway zone highlighted. The raceway is the cavity formed in the vicinity of the tuyere.

A commonly used reducing agent is pulverized coal. Pulverized coal particles have high heating rates, a short residence time in the raceway zone, and can withstand highly turbulent conditions. Because the experimental reconstruction of the raceway conditions is difficult [4], CFD can be used to test the conversion of different coals in the raceway zone virtually. Shen and Yu [5], Liu and Shen [6] and Liu et al. [7] presented studies modeling the coal as Lagrangian particles in the raceway zone. To gain useful insight in blast furnace operation through CFD, suitable models covering the essential effects of conversion need to be applied.

Many approaches to model the turbulent effects on homogeneous reactions, for example combustion reactions [8], exist. They can be applied to model the homogeneous reactions in the blast furnace and have been reviewed by Tabet and Gökalp [9]. On the contrary, the work on turbulent effects on heterogeneous reactions is relatively sparse. Some of the first attempts to study those effects have been made by Krüger et al. [10] and Haugen et al. [11]. In direct numerical simulations (DNSs) they showed that turbulence can significantly influence the mass transport to small particles and consequently reduce their conversion rate. They published a correction factor to model this effect based on the turbulent flow conditions. Later on, the work has been extended to polydisperse particle systems by Karchniwy et al. [12] and first unresolved simulation studies for industrial scale applications have

* Corresponding author.
E-mail address: eva-maria.wartha@tuwien.ac.at (E.-M. Wartha).

https://doi.org/10.1016/j.fuel.2022.125840
Received 3 June 2022; Received in revised form 19 August 2022; Accepted 23 August 2022
Available online 12 September 2022
0016-2361/© 2022 The Author(s). Published by Elsevier Ltd. This is an open access article under the CC BY license (http://creativecommons.org/licenses/by/4.0/).

Nomenclature

Acronyms

CFD	Computational Fluid Dynamics
DNS	Direct Numerical Simulation
EDC	Eddy Dissipation Concept
HCV	Higher calorific heating value
RANS	Reynolds Averaged Navier–Stokes

Greek symbols

α	mass transfer rate
$\tilde{\alpha}$	correction factor
β	mass transfer rate
δ	phase fraction
ϵ	turbulent dissipation rate, $m^2\,s^{-3}$
η	effectiveness factor
ν	viscosity, $m^2\,s^{-1}$
ω	porosity
ϕ	CO/CO_2 split factor
Φ	Thiele modulus
ρ	density, $kg\,m^{-3}$
τ	time scale, s
ξ	tortuosity

Roman symbols

$A_{1/2}$	parameters in the cluster model
A	surface area, m^2
A_g	specific internal surface area, $m^2\,kg^{-1}$
$a_{1/2}$	factor in devolatilization model
$A_{r,1/2}$	pre-exponential factor
A_{sr}	parameter for the CO/CO_2 ratio
C	diffusion constant
c	concentration, $kmol\,m^{-3}$
c_p	specific heat capacity, $J\,kg^{-1}\,K^{-1}$
Da	Damköhler number
D	Diffusion coefficient, $m^2\,s^{-1}$
d	diameter, m
$\bar{d}_{p,1}$	average diameter on number basis, m
$\bar{d}_{p,3}$	average diameter on mass basis, m
$E_{a/1/2}$	activation energy
e	emissivity
f	scattering factor
H	Latent heat, $J\,kg^{-1}$
h	retention coefficient
$I(\tilde{\alpha})$	Index as a function of $\tilde{\alpha}$
k	turbulent kinetic energy, $m^2\,s^{-2}$
k_{diff}	diffusional rate
k_{kin}	kinetic rate
$k_{L/\eta}$	wave number, m^{-1}
L	length, m
m	mass, kg
n	parameter in Rosin-Rammler dist.
n_p	particle number density
o	number of particles
p	pressure, Pa
Re	Reynolds number
R	ideal gas constant, $J\,mol^{-1}\,K^{-1}$
$RR(\tilde{\alpha})$	cumulative conversion rate
Sc	Schmidt number
Sh	Sherwood number
St	Stokes number
T	temperature, K
t	time, s
T_A	E_a/R, K
T_{sr}	parameter for the CO/CO_2 ratio
u	velocity, $m\,s^{-1}$
v	stoichiometric coefficient
W	molecular weight, $kg\,kmol^{-1}$
Y	mass fraction

Sub- & superscripts

0	initial condition/at time 0
b	bulk
chem	chemical
cl	cluster
daf	dry ash free
devol	devolatilization
eff	effective
f	fluid
gas	gaseous/molecular
g	gas
hom	homogeneous
i	iteration index (e.g. species)
Kn	Knudsen
L	integral
pore	pore
p	particles
q	quiescent
rel	relative
s	surface
t	turbulent
vol	volatiles

been presented by Karchniwy et al. [13]. Therefore, the question arises whether the conditions in the raceway are such, that the influence of turbulent clustering should be taken into account when modeling reducing agent conversion. Providing insight on these objectives is the main focus of this paper.

To ground the ensuing discussion, the necessary models to describe the thermochemical conversion process of Lagrangian particles in the blast furnace are introduced. This is followed by a recap of the correlation for the turbulent effects on the conversion by Krüger et al. [10] and Haugen et al. [11]. To obtain a better understanding of the effects, their influence is illustrated in the theoretical considerations in Section 2. We first studied the effect of the clustering in an injection rig. The particle diameter size was varied and, additionally, the importance of the gasification reactions were also investigated. Following this, the turbulent clustering effect was studied in a model of a real blast furnace, reported on in Section 3. Finally, in Section 4, we summarize our results and present concluding remarks on the importance of clustering for the coal conversion under blast furnace conditions.

2. Models and implementation

We used a finite volume approach to simulate the flow and the combustion in the domain of interest. The software OpenFOAM [14] – version 9 – was used as a basis, adding the necessary gasification and

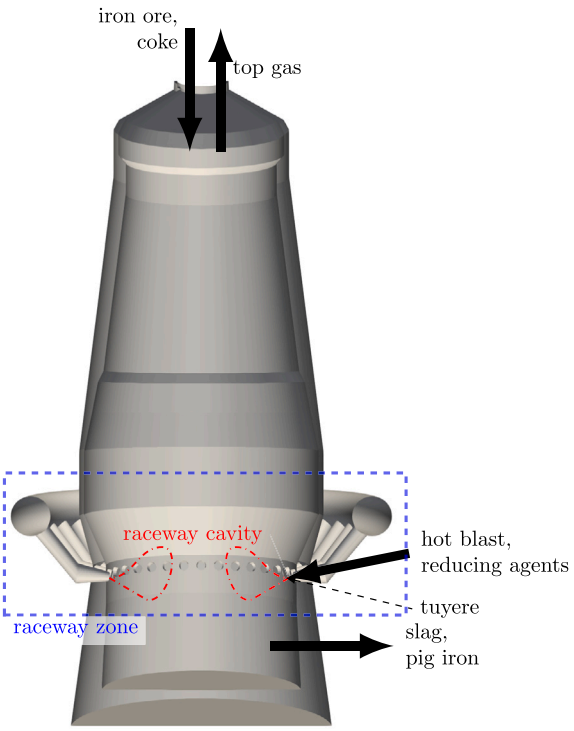

Fig. 1. Schematic description of the blast furnace with in- and outflows marked by arrows. Raceway zone is marked by dashed rectangle, two raceway cavities by dashdotted lines and tuyere position by dashed arrow.

devolatilization models and the model for the influence of turbulence on the mass transfer to the particles. The model details are discussed in the following and the code amendments for the clustering model can be found in [15].

2.1. Gas phase

Industrial processes, such as the blast furnace, are usually large in size. Therefore, the spatial resolution used in CFD is limited and the turbulence scales are not resolved on the numerical mesh. In this study, we used a Reynolds Averaged Navier–Stokes Equation (RANS)-approach to model the fluid flow in the domain of interest. A two-equation turbulence model was chosen — the k-ϵ model [16,17], which is widely applied in blast furnace simulations [9].

The gaseous phase is a multi-component mixture, which reacts with the solid particles. The volatile components are released from the solid combustion in the gas phase. The turbulent combustion process needs to be modeled by a turbulence–chemistry interaction model. We used the Eddy Dissipation Concept (EDC) from Magnussen [18], with the simplification of treating the fine structures as plug flow reactors (PFR) instead of partially stirred reactors (PSR) due to its reduced computational cost. The implications of this modeling choice have been thoroughly discussed by Ertesvåg [19] and Bösenhofer et al. [20].

To model the radiation, the P1-radiation model [21] was used. This has proven appropriate for flame simulations in conjunction with the EDC [22] and has been used for coal combustion e.g. by Tufano et al. [23]. Therefore, and because it is currently the only radiation model in OpenFOAM that can account for scattering of the Lagrangian particles, this model was chosen.

2.2. Solid particles

The combustible particles were treated as Lagrangian particles – modeled according to Newton's laws of motion. The interaction between the solid and gas phase was modeled by a drag model for the momentum (spherical drag model) and a heat transfer model [24,25] for the energy. The species and momentum equations were coupled through the source terms from the thermo-chemical conversion. The particle–particle interactions were not modeled, this means that the two-way modeling approach according to Elghobashi [26] was used. This is appropriate, since the solid phase volume fraction barely exceeds 10^{-3}. For denser particle flows four-way coupling needs to be considered. This could for example be done by using the multiphase-parcel-in-cell (MPPIC) approach, as presented by Tavakkol et al. [27].

When large numbers of particles need to be modeled it is not possible to track every single particle because of the increasing computational effort. Then, a group of particles with the same features can be lumped to a parcel. It is these parcels that are tracked in the simulation [28]. In the presented work the particles were grouped to parcels of equivalent mass.

The coal conversion was treated as a consecutive process consisting of: drying of the moist coal (vaporization of water), devolatilization, and char conversion. The modeling details of each conversion step are described in the following subsections.

2.2.1. Drying

The drying process of the coal was modeled according to:

$$\frac{dm_{\mathrm{H_2O}}}{dt} = \mathrm{Sh}\frac{D_{\mathrm{H_2O}}}{d_p}(c_{\mathrm{H_2O,s}} - c_{\mathrm{H_2O},b})\pi d_p^2 W_{\mathrm{H_2O}} \tag{1}$$

where the Sherwood correlation according to Eq. (9) was used — with the standard relative velocity u_{rel} for the particle Reynolds number, Eq (11). $D_{\mathrm{H_2O}}$ is the diffusion coefficient for water, d_p the particle diameter, $W_{\mathrm{H_2O}}$ the molecular weight of water, and $c_{\mathrm{H_2O,s}}$ and $c_{\mathrm{H_2O},b}$ the vapor concentration at the surface and in the bulk, respectively, calculated by the ideal gas law at film temperature. The binary diffusion coefficient was calculated based on the Chapman–Cowling formula [29]. For the calculation of the concentrations $c_{\mathrm{H_2O,s}}$ and $c_{\mathrm{H_2O},b}$ the saturation pressure and bulk pressure, and the mass fraction at the surface and in the bulk were used.

2.2.2. Devolatilization

A two-step kinetic model was used to model the devolatilization process above a temperature of 400 K. In this model, the release rate of volatiles for a given particle is given by:

$$\frac{dm_{\mathrm{vol}}}{dt} = \left[a_1 A_{r,1} \exp\frac{E_1}{RT} + a_2 A_{r,2} \exp\frac{E_2}{RT}\right] m_{\mathrm{vol},0} \tag{2}$$

where $m_{vol,0}$ is the initial volatile content of the particle, and $A_{r,1}, A_{r,2}$, E_1, E_2 are the kinetic parameters taken from Shen et al. [30], see Table A.3. Shen et al. [30] compared different devolatilization models for coal combustion under blast furnace conditions and concluded that this two competing step model is sufficiently accurate. The parameters α_1 and α_2 were calculated based on the volatiles content:

$$a_1 = Y_{\mathrm{vol,daf}} \qquad a_2 = 1.25a_1^2 + 0.92a_1. \tag{3}$$

The volatiles were modeled as one pseudo-species according to the elemental analysis for the coal. The thermophysical properties of that volatile species were modeled as for CH_4 and the heat balance was closed by adjusting the latent heat of devolatilization H_{devol}. The same approach was used e.g. by Petersen and Werther [31] in combination with a gasification model.

2.2.3. Char conversion

The remaining char after drying and devolatilization was modeled as carbon and ash. The carbon reacts according to the shrinking particle model [32], taking boundary diffusion limitation and kinetic limitation into account, while neglecting any pore diffusion effects, such that the conversion of char is given by:

$$\frac{dm_{\mathrm{char}}}{dt} = \eta A_p p_i \left(\frac{1}{k_{\mathrm{kin}}} + \frac{1}{k_{\mathrm{diff}}}\right)^{-1} \tag{4}$$

with the particle surface area A_p, the partial pressure of the reactant p_i, the effectiveness factor η – a model parameter – and the reaction contributions, taken as a resistance model between the kinetic reaction rate k_{kin} and the diffusion rate k_{diff}.

The kinetic reaction rate was modeled according to an Arrhenius expression:

$$k_{\text{kin}} = A_r \exp\left(-\frac{E_a}{RT}\right) \tag{5}$$

where A_r is the pre-exponential factor, E_a the activation energy, R the ideal gas constant and T the temperature, see Table A.4. The diffusion rate determined through mass transfer to the boundary was modeled as:

$$k_{\text{diff}} = \frac{C}{d_p}\left(\frac{T_p + T_f}{2}\right)^{0.75} \tag{6}$$

where C is a diffusion constant (Table A.4), d_p the particle diameter, and T_p and T_f the particle and fluid temperatures, respectively.

2.3. Turbulence effect

The models presented for the thermochemical conversion process of a coal particle are based on single particle models. Krüger et al. [10] and Haugen et al. [11] showed that small particles cluster in turbulent eddies. Consequently, since particles consume oxygen, the local oxygen concentration in the particle surroundings is typically significantly lower than the average oxygen concentration in the larger control volume. This leads to reduced mass transfer to the particle surface and consequently to reduced conversion rates.

For the derivation of the turbulence effect, several dimensionless numbers were used, which are introduced here. First, the Damköhler number, which relates the integral time scale:

$$\tau_{\text{L}} = \frac{2}{3}\frac{k}{\epsilon} \tag{7}$$

to the chemical time scale τ_{chem}:

$$\text{Da} = \frac{\tau_{\text{L}}}{\tau_{\text{chem}}} = \tau_{\text{L}}\alpha_{\text{hom,q}}. \tag{8}$$

The chemical timescale was approximated as the inverse of the reaction rate in a homogeneous quiescent flow $\alpha_{\text{hom,q}}$. Furthermore, the Sherwood number was used, which represents the rate of convective mass transfer to diffusive mass transfer. It can be expressed in analogy to the Nusselt number for heat transfer by the following correlation:

$$\text{Sh} = 2 + 0.69\text{Re}^{1/2}\text{Sc}^{1/3} \tag{9}$$

where the Schmidt number (Sc) is defined as the ratio of the viscous (dynamic viscosity ν) to the mass diffusion rate (diffusion coefficient D):

$$\text{Sc} = \frac{\nu}{D}. \tag{10}$$

Special care needs to be taken for the particle Reynolds number, because no true relative velocity exists between the velocity fluctuations of the turbulent fluid and the Lagrangian particles [11]:

$$\text{Re} = \frac{u_{\text{rel}} d_p}{\nu}. \tag{11}$$

The true relative velocity was approximated according to Haugen et al. [11]:

$$u_{\text{rel}} = \min\left(0.41\sqrt{\frac{2}{3}k}, 0.41\sqrt{\frac{2}{3}k}\left[\frac{Stk_L^{-2/3} - k_\eta^{-2/3}}{k_L^{-2/3} - k_\eta^{-2/3}}\right]\right) \tag{12}$$

including the turbulent kinetic energy k, the wave number of the integral scale

$$k_L = 2\pi\epsilon\left(\frac{3}{2k}\right)^{3/2} \tag{13}$$

and the Kolmogorov scale

$$k_\eta = 2\pi\frac{\epsilon^{0.25}}{\nu^{0.75}}. \tag{14}$$

The Stokes number

$$\text{St} = \frac{\tau_P}{\tau_L} \tag{15}$$

is the ratio of the integral to the particle time scale, where

$$\tau_p = \frac{\rho_p d_p^2}{18\nu_{\text{g}}\rho_{\text{g}}}. \tag{16}$$

Let us now turn to the actual turbulence effect on the mass transfer rate to the particles. Krüger et al. [10] proposed a correction factor to define the relationship between the reaction rate in turbulence-induced clusters, α, in relation to the reaction rate in a homogeneous quiescent flow, $\alpha_{\text{hom,q}}$:

$$\tilde{\alpha} = \frac{\alpha}{\alpha_{\text{hom,q}}}. \tag{17}$$

The reaction rate in homogeneous, quiescent flow, based on pure diffusion limitation is given as:

$$\alpha_{\text{hom,q}} = An_p k_{\text{eff}} = An_p k_{\text{diff}} \tag{18}$$

where A is the mean external surface area of the particles, n_p the particle number density and k_{eff} the effective reaction rate, which in case of diffusion limitation is equal to the diffusion rate k_{diff}.

To investigate the effect of turbulent clusters, two cases can be considered: First, for small Damköhler numbers (Eq. (8)), referred to as the individual particle combustion regime, the oxygen consumption rate scales linearly with the particle number density and is enhanced by the turbulence, scaling with the Sherwood number (Eq. (9)) as:

$$\alpha_{\text{hom,t}} = \alpha_{\text{hom,q}}\frac{\text{Sh}}{2}. \tag{19}$$

Second, for large Damköhler numbers, referred to as sheath combustion, the conversion is independent of the particle number density:

$$\alpha_{\text{cl}} = \frac{\left(A_1 A_2\right)\text{Sh}}{\tau_{\text{L}}\text{St}}. \tag{20}$$

The correlation for A_1A_2 was derived by Haugen et al. [11] as $A_1A_2 = 0.08 + \frac{St}{3}$, where St is the Stokes number (Eq. (15)) and τ_{L} is the integral time scale (Eq. (7)). The regimes for high and low Damköhler numbers were connected by taking the harmonic mean:

$$\alpha = \frac{\alpha_{\text{cl}}\alpha_{\text{hom,t}}}{\alpha_{\text{cl}} + \alpha_{\text{hom,t}}}. \tag{21}$$

Combining Eqs. (17), (19), (21), and (8) yields the correction factor, which was also obtained by Krüger et al. [10], as:

$$\tilde{\alpha} = \frac{\alpha_{\text{cl}}}{\alpha_{\text{cl}} + \text{DaSh}/\left(2\tau_{\text{L}}\right)}\frac{\text{Sh}}{2}. \tag{22}$$

The models shown were derived based on the assumption of isotropic turbulence. This was expected to be a relatively good approximation for the char conversion phase and the correlation for the clustering could be applied to RANS. Karchniwy et al. [13] presented the application of the model in RANS simulations. However, since the correlation was only applied for single particle diameters in different cases and for polydisperse particles in RANS, some clarification should be made. The Sherwood and Stokes numbers can be calculated on a particle or parcel basis, as for a single diameter. However, we suggest using averaged values on a cell basis for the Damköhler number and for the theoretical combustion in a quiescent flow. This strategy seems justifiable because Karchniwy et al. [12] showed that polydisperse particles cluster in the same regions and in a similar way. Furthermore, the Damköhler number is an average measure for the overall conversion process of the particle cloud without clustering.

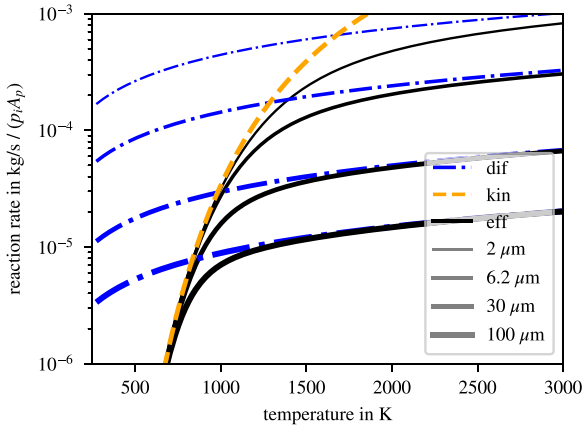

Fig. 2. Reaction rates – kinetic effect (orange), diffusional effect (blue) and effective (black) – over temperature for different particle sizes (varying line width). (For interpretation of the references to color in this figure legend, the reader is referred to the web version of this article.)

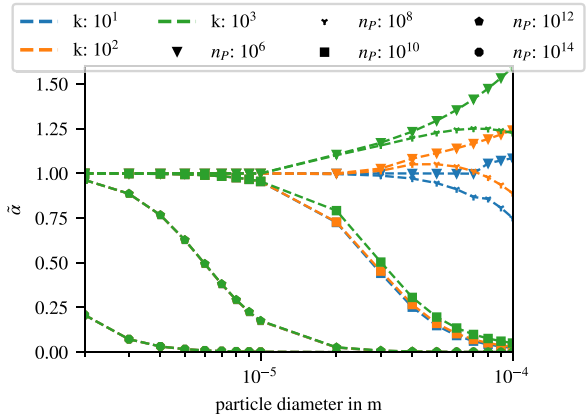

Fig. 3. Correction factor as a function of particle diameter, computed for ρ = 1300 kg m^{-3}, T = 2500 K, p = 1 bar. For the highest particle number densities ($n_p = 10^{12}, 10^{14}$) the data points are overlapping.

2.4. Theoretical considerations

If a blended reaction model as in Eq. (4) is used, the clustering only influences the mass transport to the particles and therefore only the diffusion reaction rate and not the intrinsic kinetics. Karchniwy et al. [13] showed, that even if the turbulence correction factor $\tilde{\alpha}$ is low in some cases, the clustering is less influential if the conversion is mainly controlled by kinetics. To illustrate the two regimes, Fig. 2 shows the diffusion reaction rate, the kinetic reaction rate and the effective reaction rate as a function of temperature for the char oxidation parameters used in this study (see Table A.4).

As can be seen from Fig. 2, the regime change is not only influenced by temperature, but also by the particle diameter. This is because the kinetic reaction rate is not influenced by the diameter but the diffusion rate varies with $1/d_p$. Therefore, the thermochemical conversion of smaller particles is usually less diffusion controlled. Although, specific parameters were used for Fig. 2, a kinetic-diffusion limited reaction model will always show similar characteristics.

Fig. 3 shows the correction factor $\tilde{\alpha}$ as a function of the particle diameter for a range of turbulent kinetic energy and particle number density values. The temperature was fixed to 2500 K and the particle density to 1300 kg m^{-3}, because only minor effects of those parameters were observed. The most influential parameter seems to be the particle number density. The reason for this is that for large particle number densities the chemical timescale becomes comparable to the life time of the particle clusters and eventually even larger. In the derivation it was assumed that the life time of the particle clusters is approximately equal to the turbulent time scale [11]. The volume occupied by the cluster will therefore be void of oxygen, while the surrounding volumes will contain much oxygen.

3. Results

3.1. Injection rig

To study the turbulent clustering effects on coal under raceway conditions an injection rig was first investigated. The setup was designed to resemble blast furnace conditions from Mathieson et al. [33]. A preheated coflow was injected to mimic the blast, and coal was injected through a lance inclined by 6° to resemble the injection lance in a blast furnace, see Fig. 4. The walls around the combustion chamber were insulated.

For the CFD simulation, the domain was discretized by approximately half a million, mainly hexahedral, cells using snappyHexMesh from OpenFOAM-9 [36]. The boundary conditions were set according to the experiment and are summarized in Table 1. The case setup can be found in the following repository [15]. The inlet conditions result in a pipe Reynolds number of approximately 23000. At the outlet, the pressure was set to 1 bar and Neumann boundary conditions were used for the other quantities. For the turbulent kinetic energy, a 5% turbulence intensity inlet condition was used and for the dissipation rate a turbulent mixing length model with wall function models at the wall boundaries.

Table 1
Boundary conditions for the injection rig simulations.

	Temperature	Inflow	Type
	K	Nm^3/h	
Blast	1473	300	Air
Conveying gas	298	2	N_2
Cooling gas	298	3.2	Air
Chamber walls	1800	–	–

The coal with the lowest volatile content from Shen et al. [34] was chosen to investigate the turbulence effects on char combustion. The mass flow rate of the coal is 31.6 kg h^{-1} and 10000 parcels per second were introduced in the domain. The particles were injected with an inlet velocity of 20 m s^{-1} and an initial temperature of 300 K. The proximate and ultimate analysis of the coal are given in Table A.4. The particles are reflected at the wall boundaries and the velocity is multiplied by a restitution coefficient, which was set to 0.9. Additional constant particle parameters are given in Table A.4.

Different cases were investigated to study the effect of clustering on coal conversion in the injection rig. In Section 3.1.1, we study the effect with a fixed particle diameter, equal to the mean diameter on mass basis ($\bar{d}_{p,3}$ = 30 µm) or the mean diameter on number basis ($\bar{d}_{p,1}$ = 6.2 µm). In Section 3.1.2, the case is then extended by employing a diameter distribution of the particles to compare it to the single diameter approximation. Then, the effect of turbulence on additional gasification reactions is shown in Section 3.1.3. Finally, the char conversion with a variable effectiveness factor based on the Thiele approximation is shown and compared to experimental results in Section 3.1.4.

3.1.1. Injection rig — fixed diameter

Fig. 5 shows the conversion averaged over the downstream position for the two different particle diameters. For both cases the result is plotted with the standard conversion model (“standard”) and the model including the turbulent clustering effects (“clustering”). For the larger particles $\bar{d}_{p,3}$ = 30 µm, we see a slight reduction in conversion caused

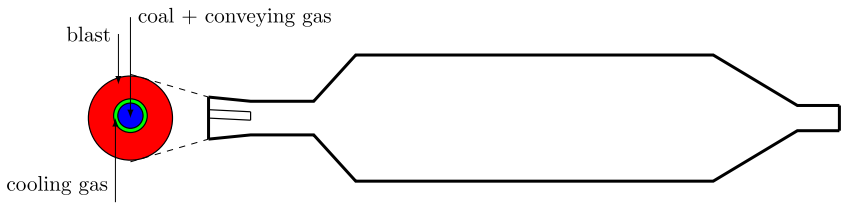

Fig. 4. Schematic drawing based on the experimental setup from Mathieson et al. [33] and publications from Shen et al. [30,34,35].

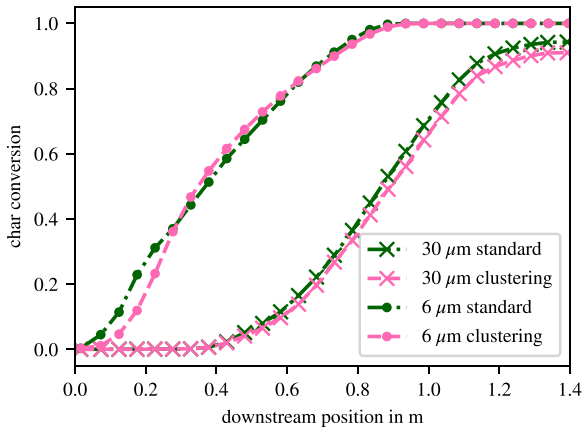

Fig. 5. Char conversion in the injection rig averaged over the downstream position for the case with particle diameter $\bar{d}_{p,3} = 30$ μm and $\bar{d}_{p,1} = 6.2$ μm.

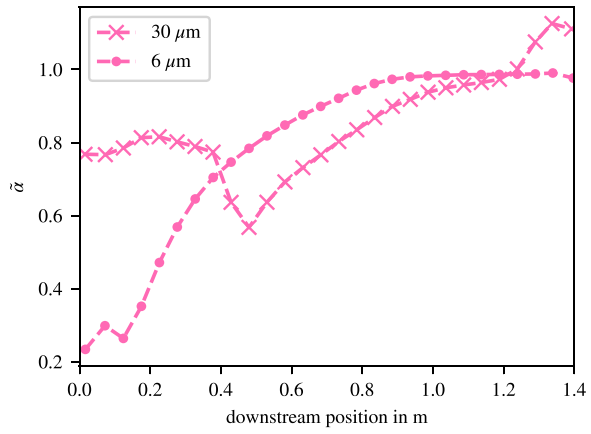

Fig. 6. Turbulence correction factor in the injection rig averaged over the downstream position for the case with particle diameter $\bar{d}_{p,3} = 30$ μm and $\bar{d}_{p,1} = 6.2$ μm.

by turbulence. This is especially pronounced in the downstream part of the rig. The results agree with the average turbulence correction factor, shown in Fig. 6, which is below one until z = 1.2 m of the domain. At the beginning, we have lower correction factors for this case, but the coal still dries and devolatizes and, therefore, no influence on the char conversion can be seen. The char conversion for the $\bar{d}_{p,3}$ = μm particles is mainly diffusion controlled, because the particles are already heated up above 1200 K when char conversion begins, as shown in Fig. 2.

For the small particles ($\bar{d}_{p,1} = 6.2$ μm), we observe a reduction in conversion at the first section (up to 0.2 m), followed by no influence of turbulence at approximately 0.4 to 0.6 m downstream. Fig. 6 shows the average turbulence correction factor, which is below 1 for the small particles in the whole domain. This confounds the observation from Fig. 5, where the conversion seems not to have been influenced or even enhanced by the turbulence for the small particles between 0.45 and 0.6 m.

Therefore, in Fig. 7 we take a closer look at the combination of the turbulence correction factor and the CO source term in the cross section of the rig. In the first part of the rig (up to 0.2 m), the turbulence correction factor is virtually everywhere well below unity, corresponding to a reduction in the conversion. Further downstream, $\tilde{\alpha}$ is still well below unity in the jet center, but approaches unity in the outer parts. This shows that for this particular case, the regions where most of the char conversion occurs are correlated with the regions where the correction factor is approaching unity. Furthermore, the overall conversion of the smaller particles is less diffusion controlled than for the larger particles, see Fig. 2, which leads overall to few turbulence effects.

To quantitatively evaluate the effect of clustering, let us organize all particles in increasing order with respect to their correction factor $\tilde{\alpha}$. The particle with the lowest correction factor is identified by the index $i = 0$ and the particle with the highest correction factor with $i = o$, where o is the total number of particles. We now define the index $I(\tilde{\alpha})$ as the index of the particle with the highest correction factor that is still below $\tilde{\alpha}$. The cumulative conversion rate $RR(\tilde{\alpha})$ to quantitatively evaluate the turbulence effect is then given by:

$$RR(\tilde{\alpha}) = \left(\sum_{i=0}^{i=I(\tilde{\alpha})} \frac{\mathrm{d}m_{\mathrm{char},i}}{\mathrm{d}t} \right) \Bigg/ \left(\sum_{i=0}^{i=o} \frac{\mathrm{d}m_{\mathrm{char},i}}{\mathrm{d}t} \right) \tag{23}$$

In Fig. 8 this cumulative conversion rate is plotted over the correction factor. The point for $RR(\tilde{\alpha}) = 50\%$ is marked by circles. This evaluation gives a better estimate of the overall turbulence influence than the average calculation of $\tilde{\alpha}$ as a function of the downstream position in Fig. 6. However, whether the conversion is diffusion or kinetic controlled will also influence the overall turbulence effect. Fig. 8 suggests that the reduction in mass transfer is stronger for the $\bar{d}_{p,1} = 6.2$ μm particles than for the $\bar{d}_{p,3} = 30$ μm particles, but it is less according to Fig. 5 because the conversion of the $\bar{d}_{p,1} = 6.2$ μm particles is less diffusion controlled than for the $\bar{d}_{p,3} = 30$ μm particles (see Fig. 2). Overall, the relation shown in Fig. 8 gives a quantitative estimate of the possible influence of turbulence, but is still dependent on the conversion regime.

3.1.2. Injection rig — diameter distribution

We now look at the effect of the particle size distribution for the same setup as studied in Section 3.1.1. The particle size distribution was fitted with a Rosin-Rammler distribution according to Maier [37] based on the experimental values reported by Shen et al. [34]. The spread parameter was fitted to $n = 0.97$ and the mean diameter was $\bar{d} = 30$ μm [37]. In real applications, and in the experiments by Shen et al. [34], coal particles are present in certain size ranges. Karchniwy et al. [12] showed that polydisperse particles experience the effects of clustering in the same way as monodisperse systems do. Therefore, the turbulence correction factor for monodispersed particles was applied directly to all the particles here.

Fig. 9 shows the overall char conversion as a function of downstream position for different size groups — comparing the standard model and the model with turbulent clustering effects. Similarly, as for the $\bar{d}_{p,3} = 30$ μm particles, the char conversion is effectively reduced through the reduced mass transfer to the clusters. Compared to the char conversion for the $\bar{d}_{p,3} = 30$ μm particles (30 μm) as shown in Fig. 5, the char conversion starts earlier and overall is slightly reduced.

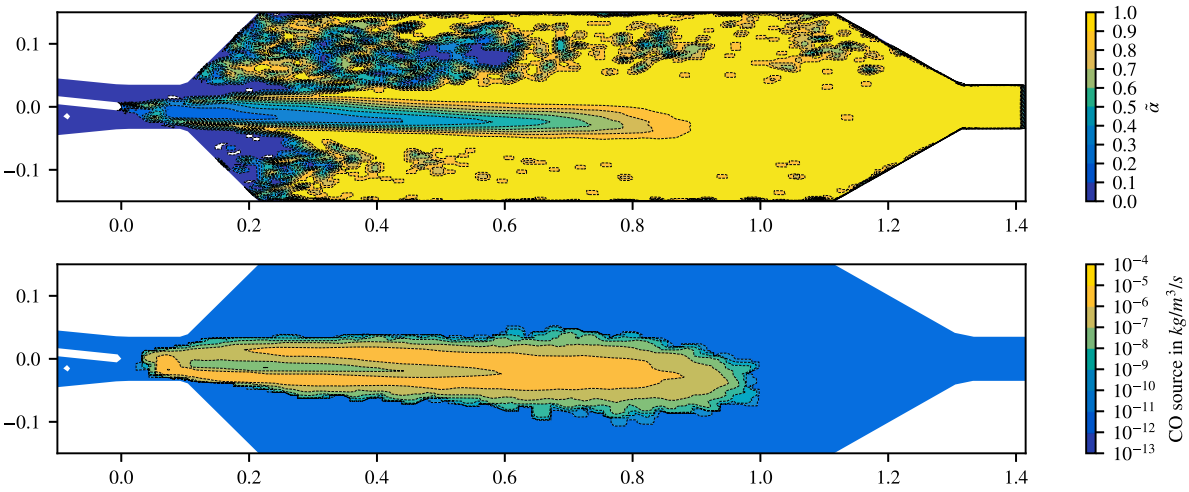

Fig. 7. The turbulence correction factor $\tilde{\alpha}$ (top) and the CO source term from char oxidation (bottom) for the simulation with $\bar{d}_{p,1} = 6.2$ µm.

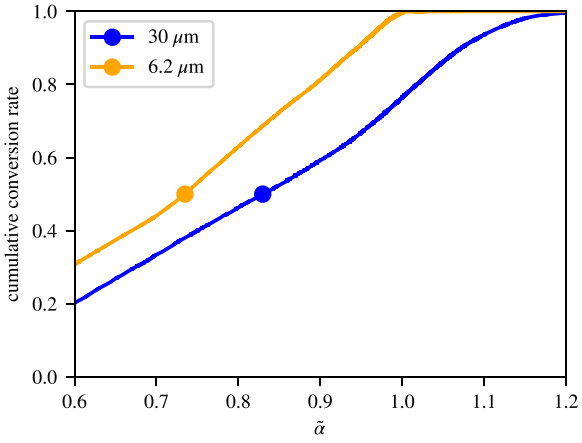

Fig. 8. Cumulative reaction rate over turbulence correction factor $\tilde{\alpha}$.

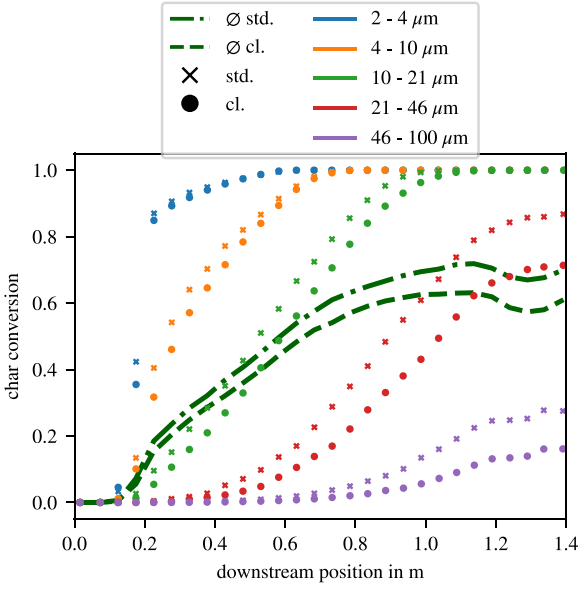

Fig. 9. Char conversion of polydisperse coal particles averaged over downstream position. The average (Ø) conversion in dashed (with clustering) and dash-dotted lines (without clustering). The conversion for different size groups are marked by circles and crosses for the standard model and model with clustering effects, respectively.

This is related to the difference in the char conversion rate for the differently sized particles. The reduction in the average conversion at approximately 1.2 m downstream might seem unreasonable at first. However, this is related to the averaging of all the particles and the fact that particles of different size hit the wall at different positions where the injection rig's cross-section is reducing. This is also undermined by the conversion rates of the grouped particles in Fig. 9. They have been grouped by size and their average conversion has been plotted. The smallest particles are converted quite fast, with only a minor influence of turbulence — similar to the $\bar{d}_{p,1} = 6.2$ µm particles before. The influence of clustering becomes more pronounced for the larger particles. The largest particles are only converted slightly before they reach the end of the injection rig. Overall, the conversion behavior and influence of clustering is similar to the conversion of the $\bar{d}_{p,3}$ particles, but also the effects of smaller and larger particles, contributing to the average char conversion marked by the green average lines in Fig. 9.

It might be striking that the char conversion decreases towards the end of the domain. This is, however, related to the averaging of the particles done over the whole cross-section. The smaller – burnt – particles are partly recirculated and therefore not transported towards the end of the domain. This is also influenced by the stronger turbulent dispersion effects on the smaller particles. Consequently, the average char conversion decreases, because the larger – partly unburnt – char particles take a greater share of the overall particles.

3.1.3. Injection rig — oxidation & gasification

In the blast furnace, besides char oxidation, gasification reactions play an important role. According to Maier [37] a kinetic-diffusion approach can be chosen to model the gasification reactions using the kinetic parameters given in Table A.4. For the effect of turbulence, the same relation, as derived by Krüger et al. [10], was used for the gasification reactions. This is justifiable since the derivation was not limited to oxidation reactions. For the H_2O and CO_2 gasification reactions, the assumption of diffusion limited reactions is reasonable for high temperature, since these reactants also need to be transported to the char surface. However, for lower temperatures and in the presence of O_2, the assumption of the model does not hold, since for these conditions CO_2 can be present right at the surface due to char oxidation. Nevertheless, for the blast furnace application the temperatures are high and, in general, the gasification reactions are mainly kinetically limited for low temperatures.

Fig. 10 shows the conversion as a function of downstream position for the diameter distribution with oxidation as well as both oxidation and gasification reactions. Naturally, the overall conversion is higher if gasification is considered. The overall trend is similar for both

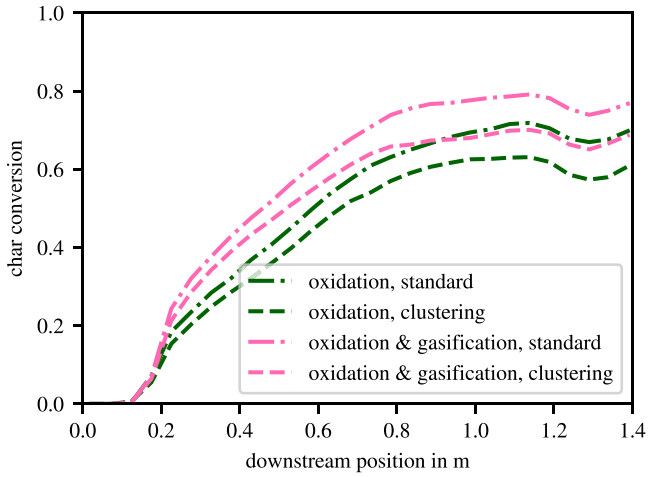

Fig. 10. Char conversion as a function of the downstream position using oxidation (green), and oxidation and gasification (pink) reactions. The results from the standard model are shown by dash-dotted lines and from the model including clustering effects with dashed lines. (For interpretation of the references to color in this figure legend, the reader is referred to the web version of this article.)

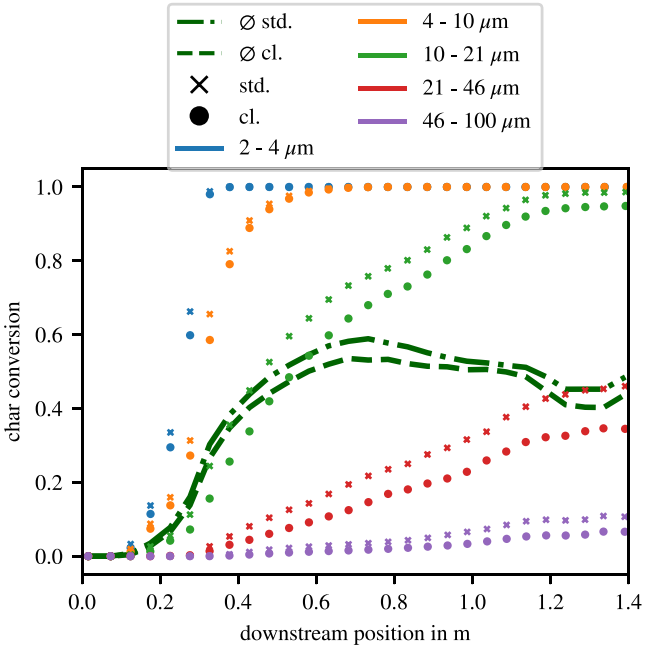

Fig. 11. Char conversion over downstream position for different diameter groups. Results from the simulation with variable effectiveness factor.

cases, but the effect of turbulence is slightly higher when gasification reactions are included. This is related to the fact that oxygen depletion plays only a minor role for the gasification reactions. This means that reactions also occur in the regions with lower turbulence correction factors. Additionally, temperatures are quite high, and therefore the gasification reactions are also partly diffusion controlled.

For simplicity, the same relation used to compute the diffusion parameter for the Schmidt number was employed for the turbulence effect for oxidation and gasification reactions. The diffusion parameter was approximated by a third order polynomial depending on temperature, based on the diffusion model for oxygen in nitrogen. The diffusional parameter is slightly different for CO_2 and H_2O. However, the differences are negligible, especially in the regimes where mass transfer is reduced by turbulence. However, if the model were applied to H_2 gasification, the differences might be significant and an independent Sherwood number should be calculated.

3.1.4. Variable effectiveness factor

Shen et al. [34] reported experimental burnout measurements for the used coal in the injection rig. To compare our simulation results to the experimental data, we need to apply the reported kinetic data for this coal. Therefore, a variable effectiveness factor is used in the following. The change of char mass is then computed as follows:

$$\frac{dm_{\text{char}}}{dt} = A_p p_i \left(\frac{1}{\eta k_{\text{kin}}} + \frac{1}{k_{\text{diff}}} \right)^{-1}. \tag{24}$$

The effectiveness factor η is taken only for the kinetic reaction rate and calculated according to the porous sphere approach, which is equivalent to Eq. (A.3) times three. The Thiele modulus is calculated as:

$$\Phi = \frac{d_P}{2} \sqrt{\frac{A_g k_{\text{kin}} p_{O_2} \rho_P \phi}{D_{\text{eff}} \rho_{O_2}}}. \tag{25}$$

To calculate the Thiele modulus, the specific internal surface area A_g is taken as 1030.57 $m^2\,kg^{-1}$, the effective diffusion rate is calculated according to Eq. (A.5) and ϕ is the split factor (Eq. (A.1)). To calculate the effective diffusion rate a porosity, ω, of 0.53, a tortuosity, ξ, of 2 and a pore radius of $4.5 \cdot 10^{-7}$ were used. The diffusion parameter for k_{diff} was changed to $5.6 \cdot 10^{-13}$ according to [34] because the effectiveness factor is now only applied to the kinetic rate.

Fig. 11 shows the char conversion for the simulation with variable effectiveness factor. Compared to the previous results, the char conversion is reduced. Additionally, we see negligible effects of clustering for particle diameters up to 10 μm.

In the experiments, the char conversion was measured at 925 mm downstream position. The experimental burnout was found to be 59.8%. At the same position the simulated burnout with the standard model is 63.3% while it is 58.4% when account is made for the effect of clustering. Both values are in a reasonable range compared to the experimentally measured burnout. The results with clustering effect underpredict the burnout a bit. However, they are closer to the experimental values then the standard model. The reported burnout from literature should be taken with care, because no error tolerance was reported and nor level of repeatability.

3.2. Blast furnace raceway

To study the effect of turbulence under real blast furnace conditions, the raceway zone of a blast furnace was simulated with pulverized coal injection. The simulation setup of the raceway is based on the work by Maier [37]. The geometry represents a 3.5 m high section of the blast furnace. An axisymmetric slice of the blast furnace raceway was chosen to reduce the computational demand. The numerical mesh of the geometry has approximately 300000 mainly hexahedral cells. In the raceway zone, not only are the blast and the reducing agents present, but also the coke supplied from the top and the liquid iron and slag. The liquid iron and slag are ignored for simplification, because they do not react in this zone [37]. Because the coke also reacts with the blast, it is also modeled as an Eulerian phase in the raceway zone. The conversion of coke is modeled by oxidation, and H_2O, H_2 and CO_2 gasification reactions. Details on the coke conversion model are given in Appendix. Validation results for this setup were presented in [38].

A hot blast mass flow of 3.554 $kg\,s^{-1}$ enters the blast furnace and forms a cavity in the coke bed. The hot blast enters with 1523 K and a mass fraction of 0.30157 O_2, 0.6946 N_2 and 0.00383 H_2O. These conditions result in a pipe Reynolds number of approximately 10^5 in the tuyere. The temperature at the bottom of the simulation domain is fixed to 1673 K and the bottom is assumed to act as a wall

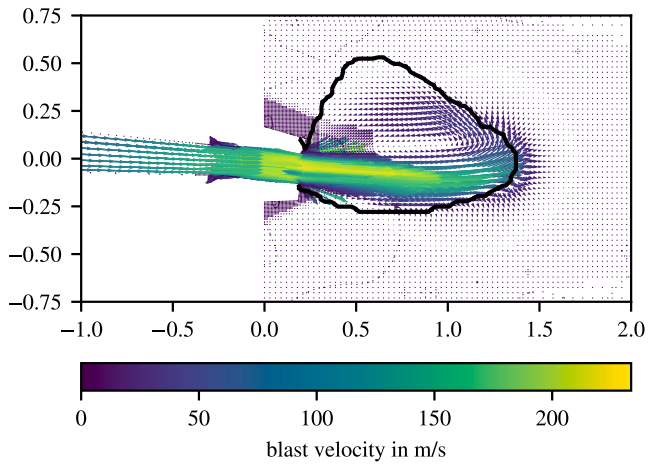

Fig. 12. Blast velocity profile in the simulated zone. The raceway cavity is marked with a solid black line. Outside the cavity, the coke bed has a porosity of 0.5.

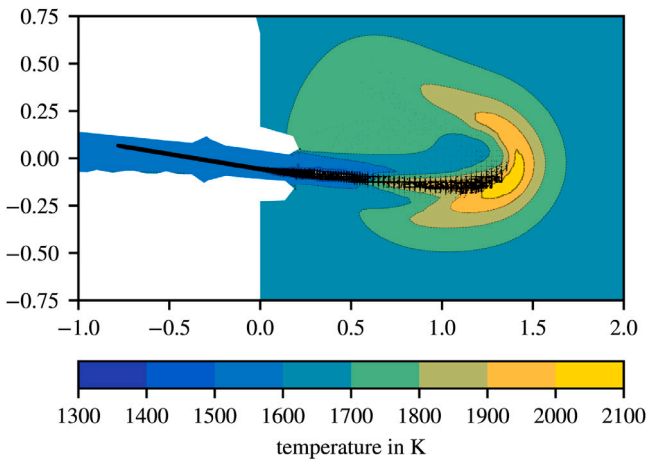

Fig. 13. Raceway with temperature distribution and pulverized coal particles.

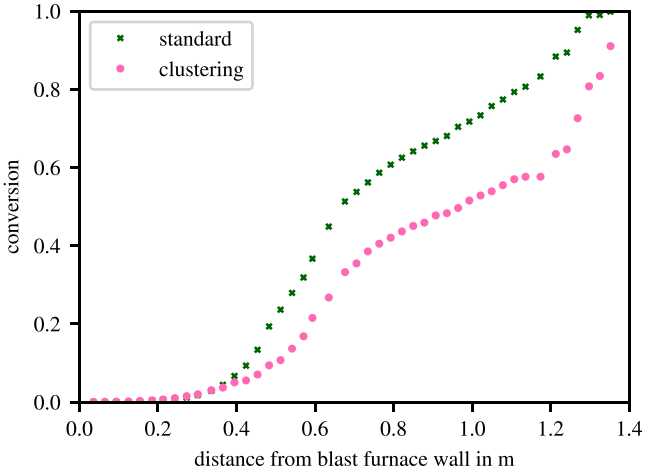

Fig. 14. Raceway with average conversion over the distance from blast furnace wall for the standard model and with clustering effect.

for the blast. The coke bed is modeled with a porosity of 0.5 and is assumed stationary. The raceway shape and size were prefixed based on the work by Maier [37], who derived the porosity profile from the results presented by Zhou [39]. In this work, we did not adapt a porosity profile, but set a fixed raceway shape with a penetration depth of 1.15 m. The raceway shape can be seen in Fig. 12. These simplifications are adequate because the focus of the current work is on the reducing agents conversion. Moreover, such simplifications speed ups have proven suitable for prediction in [37].

In Fig. 12 the blast velocity is also shown. The highest velocity occurs when the blast enters the blast furnace. The characteristic recirculation zone in the raceway can also be seen in the Figure. Close to the tuyere tip and in the raceway cavity more arrows are shown, because the mesh is refined in this region.

To study the turbulence effect on the coal conversion, 680 kg/h of the same coal as in the lab scale simulation were injected into the blast furnace. The number of parcels was set to 2000 per second. Fig. 13 shows the gas phase temperature profile in the central plane of the simulated raceway zone. The projected position of the coal particles is marked by points and scaled by their mass. The Lagrangian coal particles are deleted when they hit the stationary coke bed. This simplification is made because a lot of coal is converted before hitting the coke bed and there is a lack of validated interaction models for coke and reducing agents, therefore the interaction is often neglected, e.g. by [40].

The temperature in the beginning of the coal plume decreases first due to drying and devolatilization. In the raceway zone around the coal jet, the temperature increases due to volatile combustion and oxidation reactions. Predicting the thermal state of the lower blast furnace influenced by the pulverized coal helps to understand the influence of different coal flow rates and types on blast furnace operation [3]. According to Babich [3] the full burnout of pulverized coal within the raceway zone is hardly possible for high coal flow rates. However, an accurate prediction of the burnout helps to gain insight on the maximal possible coal rate for coke substitution.

The average char conversion of the dried and devolatilized coal particles is plotted in Fig. 14. Similar to the char conversion in the injection rig for the polydisperse particles, we see a clear reduction in conversion of the coal particles when the clustering effect is considered.

Fig. 15 shows the mass fractions of the gas species in the raceway cavity. The profiles are taken from the horizontal line starting from the middle of the tuyere at the blast furnace wall. We see that the volatile concentration is increasing from 0.5 m from the blast furnace wall. There, the coal particles devolatize and then the volatiles combust. The oxygen concentration reduces, due to volatile combustion, char oxidation and gasification reactions. The CO_2 concentration rises and reduces in the coke bed again due to the oxygen limitation. The profiles are comparable to concentrations typically found in a raceway cavity, as for example shown by Maier [37].

4. Conclusion

The presented results show that the reduction in mass transfer rate to small particles plays a crucial role under blast furnace raceway conditions. The highly turbulent flow leads to strong clustering, which is determined by the calculated correction factor $\tilde{\alpha}$. Additionally, the high temperatures lead to high kinetic rates and consequently to diffusion controlled conversion regimes. The incorporation of the model significantly influenced the overall predicted char conversion of pulverized coal particles in the raceway zone.

The correct estimation of coal conversion is important to predict the maximum possible coal flow rate and consequently the coke substitution rate. Furthermore, an accurate prediction of the coal burnout helps to estimate the thermal state of the blast furnace raceway zone which is beneficial to support process control. Additionally, further studies to substitute the coal by renewable reducing agents, such as biochar, will benefit by the inclusion of the turbulent effects on conversion. In the future, an improvement of the model by including the interactions between reducing agents and the coke bed, and a moving coke bed

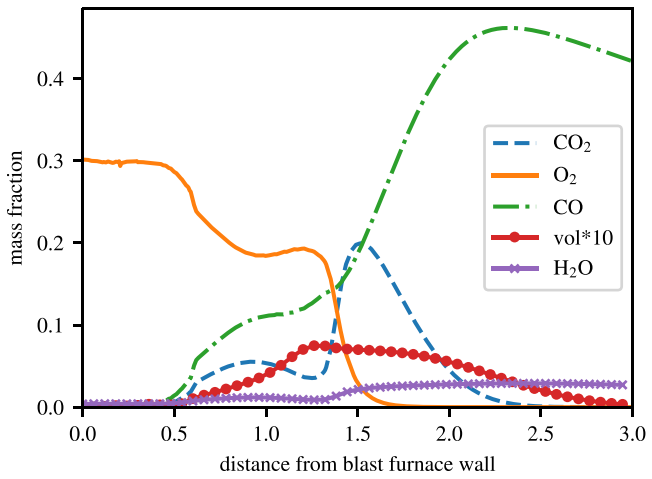

Fig. 15. Horizontal mass concentration profile from the middle of the tuyere.

could be beneficial. From a general perspective, the results indicate that an a-priori estimation through the calculation of average correction factors is impractical because the regions of correction factors have to be correlated to regions of actual reaction. Additionally, the simplified representation of small particles by particles with a mean diameter strongly influences the prediction of the correction factors and should therefore be avoided.

Finally, we would like to emphasize that the models used to account for the effect of turbulence used here, which were developed by Krüger et al. [10] and Haugen et al. [11], are based on the assumption of isotropic turbulence. This is expected to be a relatively good approximation for the char conversion phase, but care should nevertheless be taken.

CRediT authorship contribution statement

Eva-Maria Wartha: Conceptualization, Data curation, Methodology, Software, Validation, Formal analysis, Investigation, Writing – original draft, Visualization, Project administration, Funding acquisition. **Nils Erland Haugen:** Conceptualization, Data curation, Methodology, Validation, Formal analysis, Investigation, Writing – review & editing, Supervision. **Ewa Karchniwy:** Conceptualization, Data curation, Validation, Formal analysis, Investigation, Writing – review & editing. **Markus Bösenhofer:** Software, Investigation, Data curation, Writing – review & editing, Funding acquisition. **Michael Harasek:** Resources, Writing – review & editing, Supervision, Funding acquisition, Project administration. **Terese Løvås:** Conceptualization, Resources, Writing – review & editing, Supervision, Project administration.

Declaration of competing interest

The authors declare that they have no known competing financial interests or personal relationships that could have appeared to influence the work reported in this paper.

Data availability

The code is published and referenced in the manuscript.

Acknowledgments

The authors gratefully acknowledge the funding support of K1-MET GmbH, Austria, metallurgical competence center. The research program of the competence center K1-MET is supported by COMET (Competence Center for Excellent Technologies), the Austrian program for competence centers. COMET is funded by the Federal Ministry for Transport, Innovation and Technology, Austria, the Federal Ministry for Science, Research and Economy, Austria, the provinces of Upper Austria, Tyrol, and Styria, and the Styrian Business Promotion Agency, Austria. The computational results presented were achieved in part using the Vienna Scientific Cluster (VSC). The authors acknowledge TU Wien Bibliothek, Austria for financial support for editing/proofreading and through its Open Access Funding Programme. With the support of the Erasmus+ program of the European Union. The European Commission support for the production of this publication does not constitute an endorsement of the contents which reflects the views only of the authors, and the Commission cannot be held responsible for any use which may be made of the information contained therein.

Table A.2
Gas-phase reactions: Reaction rate parameters taken from Westbrook and Dryer [41] — first reaction modeled same as methane combustion.

$Vol + 2.806\,O_2 \longrightarrow CO + 4.887\,H_2O + 0.0382\,SO_2 + 0.1658\,N_2$
$CO + 0.5\,O_2 \longrightarrow CO_2$
$CO_2 \longrightarrow CO + 0.5\,O_2$

Table A.3
Devolatilization reaction: Kinetic parameters for the two-competing step devolatilization model according to [30].

	A_1	A_2	E_1	E_2
Unit	s^{-1}		$J\,kmol^{-1}$	
Value	3.7e5	1.46e13	1800	30189

Appendix. Parameters

The reaction rate parameters used in the different cases presented in this paper and details about the modeled coal are summarized here. The gas phase reactions are shown in Table A.2 based on the work from Westbrook and Dryer [41]. The parameters for the devolatilization model (Eq. (2)) are given in Table A.3.

For the coal particles studied in this paper, the proximate analysis, the ultimate analysis from Shen et al. [34] and the conversion rate parameters are summarized in Table A.4. The conversion rate parameters are given according to Eq. (4). Kinetic parameters for oxidation are from Silaen and Wang [42] and for gasification from Maier [37]. The diffusion parameter set as by Karchniwy et al. [13] and the effectiveness factors from Maier [37]. The stoichiometric coefficients for the char oxidation products ($\upsilon_{CO} = 2\frac{\phi-1}{\phi}$ and $\upsilon_{CO_2} = \frac{2-\phi}{\phi}$) are calculated as suggest by Shen et al. [34]:

$$\phi = \frac{2A_{sr}\exp\left(\frac{T_{sr}}{T_f}\right) + 2}{2 + A_{sr}\exp\left(\frac{T_{sr}}{T_f}\right)} \tag{A.1}$$

using $A_{sr} = 2500$ and $T_{sr} = 6240$ K.

For the full-scale raceway simulation, also the coke phase was included as Eulerian phase and its conversion was modeled. The effective reaction rate was computed as

$$k_{\text{eff}} = \left(\frac{1}{\beta C^{1-\upsilon}} + \frac{1}{\eta k_{\text{kin}}}\right)^{-1} C^{\upsilon}. \tag{A.2}$$

Where k_{kin} is the kinetic reaction rate modeled according to Arrhenius with the parameters given in Table A.5 and β the mass transfer rate through the boundary layer. The effectiveness factor η accounts for pore diffusion and is modeled according to Liu and Niksa [45]:

$$\eta = \frac{1}{\Phi}\left(\frac{1}{\tanh\Phi} - \frac{1}{\Phi}\right) \tag{A.3}$$

Table A.4
Proximate analysis in mass-%, ultimate analysis, particle parameters and reaction rate parameters.

Moisture	vol.	ash	fixed c.	HCV
%	%	%	%	$MJ\,kg^{-1}$
0.9	12.4	8	78.7	32.98
Elemental analysis in mass-%				
C	H	N	S	O
91.3	4	1.9	0.5	2.3
Constant particle parameters				
e	f	h	ρ_p	c_p
–	–	–	$kg\,m^{-3}$	$J\,kg^{-1}\,K^{-1}$
0.9	0.5	0.3	1300	1500
Reaction rate parameters				
	A_r	E_a	C	η
	$s\,m^{-1}$	$J\,kmol^{-1}$	$s\,K^{-\frac{3}{4}}$	–
oxid.	0.052	$6.1 \cdot 10^7$	$5 \cdot 10^{-12}$	0.6
CO_2 gasif.	20230	$3.304 \cdot 10^8$	$5 \cdot 10^{-12}$	0.7
H_2O gasif.	606.9	$2.697 \cdot 10^8$	$5 \cdot 10^{-12}$	0.6

Table A.5
Reaction parameters for coke conversion. Parameters for oxidation and CO_2 conversion from Rumpel [43] and for H_2O conversion from Tepper [44].

Reaction	A_E	E_a/R	υ
$coke + 1.0475\,O_2 \longrightarrow CO_2 + 0.146\,H_2O$	4.8e9	16731	0.59
$coke + 0.949\,H_2O \longrightarrow CO + 1.095\,H_2$	3.54	15600	1
$coke + CO_2 \longrightarrow 2\,CO + 0.051\,H_2O + 0.095\,H_2$	2.7e5	18520	0.13

Table A.6
Particle properties for the coke modeled as Eulerian phase in the blast furnace.

ω	ξ	d_{pore}
0.41	3.7	2e−7

with the Thiele modulus Φ from [46]:

$$\Phi = \frac{d_p}{2}\sqrt{\frac{1+\upsilon}{2}\frac{k_{kin}\rho_p c^{\upsilon-1}}{D_{eff}}}. \tag{A.4}$$

To calculate the Thiele modulus, the particle diameter d_p, the kinetic reaction rate k_{kin}, the particle density ρ_p, the concentration of the gaseous component c with its coefficient υ and the effective diffusion coefficient D_{eff} were used. The diffusion coefficient is calculated based on the Knudsen D_{Kn} [47], pore Diffusion D_{gas} [29] and the ratio of porosity ω and tortuosity ξ (see Table A.6):

$$D_{eff} = \left(\frac{1}{D_{Kn}} + \frac{1}{D_{gas}}\right)^{-1}\frac{\omega}{\xi}. \tag{A.5}$$

The mass transfer through the boundary layer is modeled as follows:

$$\beta = \frac{Sh D_{gas}}{d_P} A_p \tag{A.6}$$

with the Sherwood correlation from [48]:

$$Sh = \frac{0.375}{1-\delta_{coke}} Re^{0.641} Sc^{\frac{1}{3}}. \tag{A.7}$$

References

[1] Commission of the European Communities. Commission staff working document: Towards competitive and clean European steel. Tech. rep., Commission of the Eueropean Communities; 2021.

[2] Babich A, Senk D. Coal use in iron and steel metallurgy. In: The coal handbook: Towards cleaner production, vol. 2, Woodhead Publishing Limited; 2013, p. 267–311. http://dx.doi.org/10.1533/9781782421177.3.267.

[3] Babich A. Blast furnace injection for minimizing the coke rate and CO2 emissions. Ironmak Steelmak 2021;1–14. http://dx.doi.org/10.1080/03019233.2021.1900037.

[4] Bösenhofer M, Wartha E-M, Jordan C, Feilmayr C, Stocker H, Hauzenberger F, et al. Suitability of pulverised coal testing facilities for blast furnace applications. Ironmak Steelmak 2020;47(5). http://dx.doi.org/10.1080/03019233.2019.1565152.

[5] Shen Y, Yu A. Characterization of coal burnout in the raceway of an ironmaking blast furnace. Steel Res Int 2015;86(6):604–11. http://dx.doi.org/10.1002/srin.201400333.

[6] Liu Y, Shen Y. Combined experimental and numerical study of charcoal injection in a blast furnace: Effect of biomass pretreatment. Energy Fuels 2020;34(1):827–41. http://dx.doi.org/10.1021/acs.energyfuels.9b02949.

[7] Liu L, Kuang S, Jiao L, Guo B, Yu A. Optimization of pulverized coal injection (PCI) rate in an ironmaking blast furnace by an integrated process model. Fuel 2021;(October):122832. http://dx.doi.org/10.1016/j.fuel.2021.122832.

[8] Veynante D, Vervisch L. Turbulent combustion modeling. Prog Energy Combust Sci 2002;28(3):193–266. http://dx.doi.org/10.1016/S0360-1285(01)00017-X.

[9] Tabet F, Gökalp I. Review on CFD based models for co-firing coal and biomass. Renew Sustain Energy Rev 2015;51:1101–14. http://dx.doi.org/10.1016/j.rser.2015.07.045.

[10] Krüger J, Haugen NEL, Løvås T. Correlation effects between turbulence and the conversion rate of pulverized char particles. Combust Flame 2017;185:160–72. http://dx.doi.org/10.1016/j.combustflame.2017.07.008.

[11] Haugen NEL, Krüger J, Mitra D, Løvås T. The effect of turbulence on mass transfer rates of small inertial particles with surface reactions. J Fluid Mech 2018;836:932–51. http://dx.doi.org/10.1017/jfm.2017.820.

[12] Karchniwy E, Klimanek A, Haugen NEL. The effect of turbulence on mass transfer rates between inertial polydisperse particles and fluid. J Fluid Mech 2019;874(x):1147–68. http://dx.doi.org/10.1017/jfm.2019.493.

[13] Karchniwy E, Haugen NEL, Klimanek A, Langørgen Ø, Sładek S. The effect of turbulence on mass transfer in solid fuel combustion: RANS model. Combust Flame 2021;227:65–78. http://dx.doi.org/10.1016/j.combustflame.2020.12.040.

[14] Weller HG, Tabor G, Jasak H, Fureby C. A tensorial approach to computational continuum mechanics using object-oriented techniques. Comput Phys 1998;12(6):620–31. http://dx.doi.org/10.1063/1.168744.

[15] clusterCloud. 2022. http://dx.doi.org/10.5281/zenodo.6579850.

[16] Jones WP, Launder BE. The prediction of laminarization with a two-equation model of turbulence. Int J Heat Mass Transfer 1972;15:301–14.

[17] Launder BE, Spalding DB. The numerical computation of turbulent flows. Comput Methods Appl Mech Engrg 1974;3:269–89. http://dx.doi.org/10.1016/0045-7825(74)90029-2.

[18] Magnussen BF. The Eddy dissipation concept a bridge between science and technology. In: ECCOMAS thematic conference on computational combustion. 2005.

[19] Ertesvåg IS. Analysis of some recently proposed modifications to the eddy dissipation concept (EDC). Combust Sci Technol 2020;192(6):1108–36. http://dx.doi.org/10.1080/00102202.2019.1611565.

[20] Bösenhofer M, Wartha E-M, Jordan C, Harasek M. The eddy dissipation concept-analysis of different fine structure treatments for classical combustion. Energies 2018;11(7). http://dx.doi.org/10.3390/en11071902.

[21] Siegel R, Howell JR. Thermal radiation heat transfer III radiation transfer with absorbing, emitting, and scattering media, vol. III. National Aeronatics and Space Administration; 1971, URL http://ntrs.nasa.gov/archive/nasa/casi.ntrs.nasa.gov/19710021465.pdf.

[22] De A, Oldenhof E, Sathiah P, Roekaerts D. Numerical simulation of Delft-Jet-in-Hot-Coflow (DJHC) flames using the eddy dissipation concept model for turbulence-chemistry interaction. Flow Turbul Combust 2011;87(4):537–67. http://dx.doi.org/10.1007/s10494-011-9337-0.

[23] Tufano GL, Stein OT, Wang B, Kronenburg A, Rieth M, Kempf AM. Coal particle volatile combustion and flame interaction. Part I: Characterization of transient and group effects. Fuel 2018;229(May):262–9. http://dx.doi.org/10.1016/j.fuel.2018.02.105.

[24] Ranz WEE, Marshall WRJR. Evaporation from drops Part I. Chem Eng Prog 1952;48(3):141–6.

[25] Ranz WE, Marshall WRJR. Evaporation from drops: Part II. Chem Eng Prog 1952;48(4):173–80.

[26] Elghobashi S. An updated classification map of particle-laden turbulent flows. In: IUTAM symposium on computational approaches to multiphase flow. Fluid mechanics and its applications, vol. 81, 2006, p. 3–10. http://dx.doi.org/10.1007/1-4020-4977-3_1.

[27] Tavakkol S, Zirwes T, Denev JA, Jamshidi F, Weber N, Bockhorn H, et al. An Eulerian-Lagrangian method for wet biomass carbonization in rotary kiln reactors. Renew Sustain Energy Rev 2021;139(March):110582. http://dx.doi.org/10.1016/j.rser.2020.110582.

[28] Jakobsen HA. Chemical reactor modeling. 2008.

[29] Hishida M, Hayashif AK. Numerical simulation of pulsed Jet Plume combustion. Dyn Heterog Combust React Syst 1993;343–61. http://dx.doi.org/10.2514/5.9781600866258.0343.0361.

[30] Shen YS, Guo B, Yu A, Maldonado D, Austin P, Zulli P. Three-dimensional modelling of coal combustion in blast furnace. ISIJ Int 2008;48(6):777–86. http://dx.doi.org/10.2355/isijinternational.48.777.
[31] Petersen I, Werther J. Experimental investigation and modeling of gasification of sewage sludge in the circulating fluidized bed. Chem Eng Process 2005;44(7):717–36. http://dx.doi.org/10.1016/j.cep.2004.09.001.
[32] Yagi BS, Kunii D. Combustion of solids. Symp Int Combust 1955;5(1):231–44. http://dx.doi.org/10.1016/S0082-0784(55)80033-1.
[33] Mathieson JG, Truelove JS, Rogers H. Toward an understanding of coal combustion in blast furnace tuyere injection. Fuel 2005;84(10):1229–37. http://dx.doi.org/10.1016/j.fuel.2004.06.036.
[34] Shen YS, Maldonado D, Guo BY, Yu AB, Austin P, Zulli P. Computational fluid dynamics study of pulverized coal combustion in blast furnace raceway. Ind Eng Chem Res 2009;48(23):10314–23. http://dx.doi.org/10.1021/ie900853d.
[35] Shen YS, Guo BY, Yu AB, Zulli P. A three-dimensional numerical study of the combustion of coal blends in blast furnace. Fuel 2009;88(2):255–63. http://dx.doi.org/10.1016/j.fuel.2008.08.013.
[36] OpenFOAM Foundation. OpenFOAM-9. 2021, URL https://github.com/OpenFOAM/OpenFOAM-9.
[37] Maier C. Numerical modeling of the blast furnace process injection of auxiliary reducing agents into the raceway (Dissertation), Technische Universität Wien; 2015, http://dx.doi.org/10.34726/hss.2015.14843.
[38] Wartha E-M, Bösenhofer M, Hauzenberger F, Stocker H, Feilmayr C, Harasek M. Influence of raceway shape on species concentration. In: AISTech - Iron and steel technology conference proceedings. Pittsburgh, 2022.
[39] Zhou CQ. CFD Modeling for high rate pulverized Coal injection (PCI) to blast furnaces. Tech. rep., U.S. Department of Energy; 2008.
[40] Shen YS, Guo BY, Yu AB, Austin PR, Zulli P. Three-dimensional modelling of in-furnace coal/coke combustion in a blast furnace. Fuel 2011;90(2):728–38. http://dx.doi.org/10.1016/j.fuel.2010.08.030.
[41] Westbrook CK, Dryer FL. Simplified reaction mechanisms for the oxidation of hydrocarbon fuels in flames. Combust Sci Technol 1981;27(1–2):31–43. http://dx.doi.org/10.1080/00102208108946970.
[42] Silaen A, Wang T. Comparison of Instantaneous, equilibrium, and finite-rate gasification models in an entrained-flow coal gasifier. In: Proceedings of the 26th international Pittsburgh coal conference. 2009.
[43] Rumpel S. Die autotherme Wirbelschichtpyrolyse zur Erzeugung heizwertreicher Stützbrennstoffe (Ph.D. thesis), Universität Karlsruhe; 2000.
[44] Tepper H. Zur Vergasung von Rest- und Abfallholz in Wirbelschichtreaktoren für dezentrale Energieversorgungsanlagen (Dissertation), Otto-von-Guericke-Universität Magdeburg; 2005, p. 1–176.
[45] Liu GS, Niksa S. Coal conversion submodels for design applications at elevated pressures. Part II. Char gasification. Prog Energy Combust Sci 2004;30:679–717. http://dx.doi.org/10.1016/j.pecs.2004.08.001.
[46] Thiele EW. Relation between catalytic activity and size of particle. Ind Eng Chem 1939;31(7):916–20. http://dx.doi.org/10.1021/ie50355a027.
[47] Szekely J, Evans JW, Sohn HY. Gas-solid reactions. Inc.: Academic Press; 1976.
[48] Petrovic LJ, Thodos G. Mass transfer in flow of gases through packed beds. Low Reynolds number region. Ind Eng Chem Fundam 1968;7(2):274–80.